Advances in Water Resources 33 (2010) 419–429

Contents lists available at ScienceDirect

Advances in Water Resources

journal homepage: www.elsevier.com/locate/advwatres

An analytical solution for heterogeneous and anisotropic anticline reservoirs under well injection

Hund-Der Yeh [a,*], Chia-Chen Kuo [a,b]

[a] Institute of Environmental Engineering, National Chiao Tung University, Hsinchu 300, Taiwan
[b] National Center for High-Performance Computing, National Applied Research Laboratories, Hsinchu 300, Taiwan

ARTICLE INFO

Article history:
Received 1 April 2009
Received in revised form 27 January 2010
Accepted 27 January 2010
Available online 2 February 2010

Keywords:
Aquifer
Analytical model
Anisotropic
Heterogeneous
Irregular boundary
Well injection

ABSTRACT

This study develops a mathematical model for describing the steady-state head response to fluid injection into a fully penetrating well in a heterogeneous and anisotropic anticline reservoir. In the model, the upper boundary of the anticline reservoir is approximated by a form of step change in reservoir thickness and the domain of the reservoir is divided into two regions with different hydraulic conductivities. By virtue of the properties of Fourier series, the method of separation of variables is employed to develop the analytical solution of the model.

This new solution can be applied to estimating head distributions or injection rates for various geometrical conditions of the reservoir. If the trap is absent, the solution can be utilized to analyze head distributions in the reservoir system with two concentric transmissivity zones. Moreover, if the upper boundary becomes flat and the reservoir is homogeneous and isotropic, the solution reduces to the Thiem equation.

1. Introduction

An anticline reservoir has long been known to play an important role in subsurface recharge and waste disposal [1]; thus, the study of well-flow systems in anticline formations is essential. For example, the Chingtsaohu anticline under the Toukoshan formation of northern Taiwan was assessed as a candidate for groundwater recharge [2] and the Chinshui anticline was regarded as a host formation for CO_2 sequestration [3].

Al-Mohannadi et al. [4] pointed out the lack of literature support for analyzing the impact of curve boundaries due to anticline structures on well injection or production. They therefore built a finite-difference model to investigate the behavior of unsteady state flow for a horizontal well in anticline reservoirs. Saripalli et al. [5] developed a well injectivity decline simulator to simulate well performance during deep-well injection of municipal and industrial wastes as well as liquid hazardous wastes. Though several analytical models for well-injection problems had been reported (e.g., [6,7]), the shape of the host formation was however limited to be flat. The development of a mathematical model to simulate the head distribution for well injection into anticline reservoirs is therefore needed.

Kirkham [8] developed a methodology for describing the flow of a well partially penetrating a uniform confined aquifer. He proposed an efficient approach using domain partition to deal with a mixed boundary value problem and developed a steady-state solution to problems of flow into a partial penetrating well. The critical step leading to the analytical expression was to divide the target field into two regions with a virtual interface satisfying the hydraulic continuity requirements between individual ones. Javandel and Zaghi [9] adopted a domain partition procedure similar to that given by Kirkham [8] and developed an analytical solution for steady-state flow in a uniform confined aquifer fully penetrated by a well with bottom extensions.

The objective of this paper is to develop a mathematical model for predicting the steady-state head response to fluid injection in an anticline reservoir while maintaining a constant head at the fully penetrating well. The steady-state model has the advantages that the solution of the model can be applied to estimating the head distribution easily and assessing long-term injection operation. The anticline reservoir is thought to have a finite remote boundary as well as heterogeneous and anisotropic hydraulic conductivity. When developing the analytical solution of the model, the upper boundary of anticline reservoir is approximated by a form of step change in reservoir thickness. The whole domain of the reservoir with an irregular boundary is then split into two regions; each region has its own hydraulic conductivity. By virtue of the properties of Fourier series [10], the method of separation of variables is employed to develop the analytical expression of the model. This new solution can be utilized to predict the steady-state head distribution after fluid injection into anticline

* Corresponding author. Tel.: +886 3 5731910; fax: +886 3 5725958.
E-mail address: hdyeh@mail.nctu.edu.tw (H.-D. Yeh).

0309-1708/$ - see front matter © 2010 Elsevier Ltd. All rights reserved.
doi:10.1016/j.advwatres.2010.01.007

Nomenclature

a_0	constant used in (11) and (12)
a_m	constants used in (11)
b_n	constants used in (12)
$\tilde{c}_1,\ \tilde{c}_2$	constants used in (17)
h_i	hydraulic heads used in (1)
h_1	hydraulic head of region 1
h_2	hydraulic head of region 2
h_o	hydraulic head at the outer boundary
h_w	hydraulic head at the wellbore
$\Delta h = h_o - h_w$	difference between the heads at the injection well and outer boundary
I_0	modified Bessel function of the first kind of order zero
I_1	modified Bessel function of the first kind of order one
K_0	modified Bessel function of the second kind of order zero
K_1	modified Bessel function of the second kind of order one
Q_f	volumetric flow rate for flat reservoir with heterogeneous but isotropic conductivity defined by (40)
Q_h	volumetric flow rate for anticline reservoir with homogeneous and isotropic conductivity defined by (39)
Q_o	volumetric flow rate for flat reservoir with homogeneous and isotropic conductivity defined by (41)
Q_w	volumetric flow rate for anticline reservoir with heterogeneous and anisotropic conductivity defined by (38)
r	radial coordinate
r_1	distance from the center of the injection well to the interface between regions 1 and 2 (trap width)
r_2	distance from the center of the injection well to the outer boundary where the head change is negligible
r_w	well radius
$V_1,\ V_2$	volumes bounded by the upper boundary and its approximate form of step change in reservoir thickness as shown in Fig. 1
z	vertical coordinate
z_1	aquifer thickness of region 1
z_2	aquifer thickness of region 2
z_f	uniform aquifer thickness ($z_f = z_1 = z_2$)
z_δ	trap height $z_1 - z_2$
α_j	constants defined by (33)
β_{jm}	constants defined by (34)
$\xi_m,\ \eta_n$	constants used in (18)
κ_{ri}	horizontal hydraulic conductivities where i = 1 for region 1 and i=2 for region 2
κ_{zi}	vertical hydraulic conductivities where i = 1 for region 1 and i=2 for region 2
κ_h	homogeneous and isotropic hydraulic conductivity
λ_1	$m\pi/z_1$
λ_2	$n\pi/z_2$
τ_0	function of I_0 and K_0 defined by (13)
τ_1	function of $I_0,\ I_1,\ K_0$ and K_1 defined by (19)
ω_0	function of I_0 and K_0 defined by (14)
ω_1	function of $I_0,\ I_1,\ K_0$ and K_1 defined by (20)
Γ_j	constants defined by (23)
Λ_{nm}	constants defined by (30) and (31)
Θ_{jn}	constants defined by (24) and (25)
∇^2	Laplacian operator

reservoirs or to design the injection rate of anticline reservoirs for long-term operation.

2. Mathematical model

2.1. Governing equation and corresponding boundary conditions

Fig. 1 illustrates the schematic representation of a heterogeneous and isotropic confined aquifer with an injection well. The upper boundary of the aquifer is convex upward and this aquifer is thus regarded as an anticline reservoir. The well, located right at the crest of the reservoir, with a radius of r_w penetrates fully into the reservoir. Consider that the reservoir, formed by compression, has different hydraulic conductivities for the regions near the crest and some distance away from the crest. Thus, the upper boundary is approximated by a form of step change represented by the dashed line shown in Fig. 1. Note that the new boundary should ensure that the new reservoir volume remains the same as that before approximation, i.e., $V_1 = V_2$ as shown in the figure. In addition, the location of abrupt change in the shape is taken as a divide for the formation conductivity.

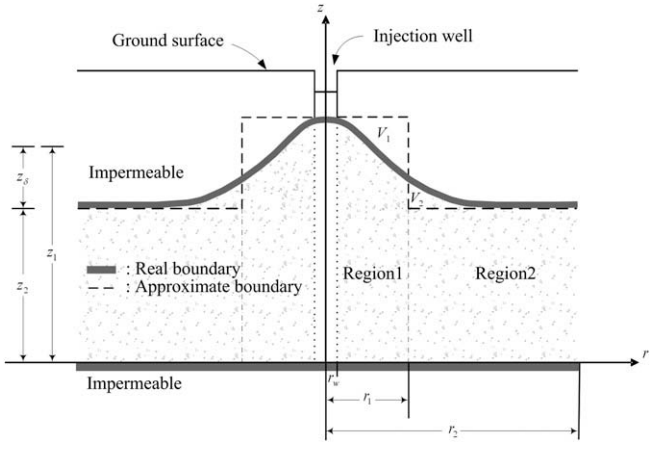

Fig. 1. Schematic representation of an anticline reservoir.

Region 1, with hydraulic conductivities κ_{r1} and κ_{z1}, has an area bounded by $r_w < r < r_1$ and $0 < z < z_1$ while the area of region 2, with hydraulic conductivities κ_{r2} and κ_{z2}, is bounded by $r_1 < r < r_2$ and $0 < z < z_2$. The hydraulic heads at the wellbore and at r_2 are maintained as constants h_w and h_o, respectively. The variable r_1 denotes the distance from the center of the well to the interface of the two regions while r_2 represents the distance from the center of the well to the outer boundary [11,12].

The steady-state head distributions h_i in both regions with anisotropic formation can be described as

$$\frac{\kappa_{ri}}{r}\frac{\partial}{\partial r}\left(r\frac{\partial h_i}{\partial r}\right) + \kappa_{zi}\frac{\partial^2 h_i}{\partial z^2} = 0 \quad \text{for } i = 1, 2. \tag{1}$$

The appropriate boundary conditions for Eq. (1) are as follows:

$$h_1(r_w, z) = h_w \quad \text{for } 0 \leqslant z \leqslant z_1, \tag{2}$$

$$\frac{\partial h_1(r,0)}{\partial z} = 0 \quad \text{for } r_w \leqslant r \leqslant r_1, \tag{3}$$

$$\frac{\partial h_1(r,z_1)}{\partial z} = 0 \quad \text{for } r_w \leqslant r \leqslant r_1, \tag{4}$$

$$h_2(r_2, z) = h_o \quad \text{for } 0 \leqslant z \leqslant z_2, \tag{5}$$

$$\frac{\partial h_2(r,0)}{\partial z} = 0 \quad \text{for } r_1 \leqslant r \leqslant r_2, \tag{6}$$

$$\frac{\partial h_2(r,z_2)}{\partial z} = 0 \quad \text{for } r_1 \leqslant r \leqslant r_2. \tag{7}$$

At r_1, there are three conditions. First, a no-flow condition at the upper right part of region 1 is imposed as:

$$\kappa_{r1}\frac{\partial h_1(r_1,z)}{\partial r}=0 \quad \text{for } z_2\leqslant z\leqslant z_1. \tag{8}$$

Moreover, the continuity requirements for the head and flux at the interface are respectively

$$h_1(r_1,z)=h_2(r_1,z) \quad \text{for } 0\leqslant z\leqslant z_2 \tag{9}$$

and

$$\kappa_{r1}\frac{\partial h_1(r_1,z)}{\partial r}=\kappa_{r2}\frac{\partial h_2(r_1,z)}{\partial r} \quad \text{for } 0\leqslant z\leqslant z_2. \tag{10}$$

2.2. Development of solutions for hydraulic head distribution in regions 1 and 2

The method of separation of variables is adopted to solve Eq. (1) along with Eqs. (2)–(7). The detailed development for the hydraulic head distribution solutions in regions 1 and 2 with unknown coefficients a_0, a_m, and b_n is given in Appendix A and the results for these two regions are respectively

$$h_1=h_w-a_0\frac{\ln(r_w/r)}{\ln(r_w/r_1)}-\sum_m a_m\tau_0\left(\sqrt{\frac{\kappa_{z1}}{\kappa_{r1}}}\lambda_1 r\right)\cos(\lambda_1 z) \tag{11}$$

and

$$h_2=h_o-(a_0+\Delta h)\frac{\ln(r_2/r)}{\ln(r_2/r_1)}-\sum_n b_n\omega_0\left(\sqrt{\frac{\kappa_{z2}}{\kappa_{r2}}}\lambda_2 r\right)\cos(\lambda_2 z), \tag{12}$$

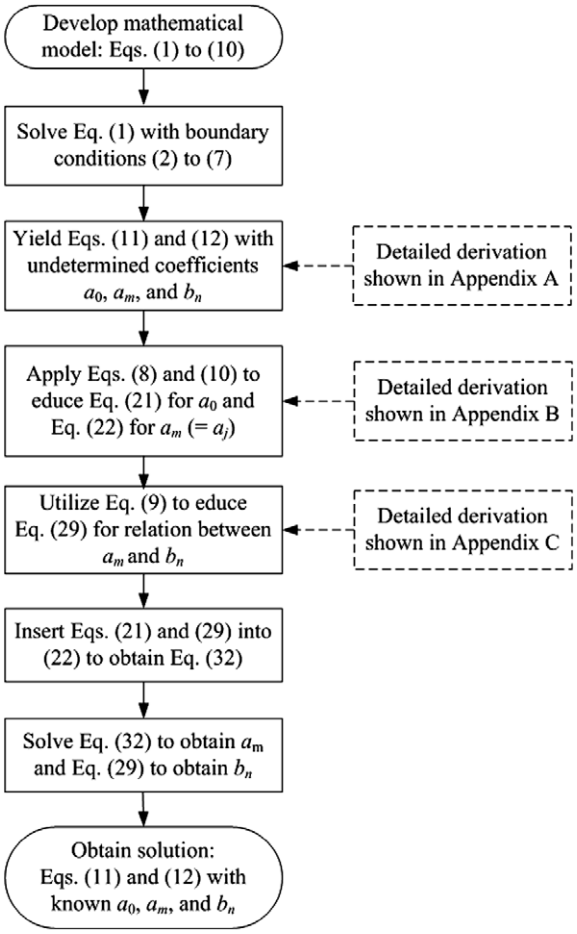

Fig. 2. Flowchart to illustrate the solution procedure.

where $\lambda_1=m\pi/z_1$ and $\lambda_2=n\pi/z_2$; m and n are positive integers (i.e., 1,2,3,...); Δh represents the difference between the heads at the injection well and outer boundary; τ_0 and ω_0 are lumped parameters respectively defined as

$$\tau_0(\lambda_1 r)=\frac{K_0\left(\sqrt{\frac{\kappa_{z1}}{\kappa_{r1}}}\lambda_1 r\right)I_0\left(\sqrt{\frac{\kappa_{z1}}{\kappa_{r1}}}\lambda_1 r_w\right)-I_0\left(\sqrt{\frac{\kappa_{z1}}{\kappa_{r1}}}\lambda_1 r\right)K_0\left(\sqrt{\frac{\kappa_{z1}}{\kappa_{r1}}}\lambda_1 r_w\right)}{K_0\left(\sqrt{\frac{\kappa_{z1}}{\kappa_{r1}}}\lambda_1 r_1\right)I_0\left(\sqrt{\frac{\kappa_{z1}}{\kappa_{r1}}}\lambda_1 r_w\right)-I_0\left(\sqrt{\frac{\kappa_{z1}}{\kappa_{r1}}}\lambda_1 r_1\right)K_0\left(\sqrt{\frac{\kappa_{z1}}{\kappa_{r1}}}\lambda_1 r_w\right)} \tag{13}$$

and

$$\omega_0(\lambda_2 r)=\frac{K_0\left(\sqrt{\frac{\kappa_{z2}}{\kappa_{r2}}}\lambda_2 r\right)I_0\left(\sqrt{\frac{\kappa_{z2}}{\kappa_{r2}}}\lambda_2 r_2\right)-I_0\left(\sqrt{\frac{\kappa_{z2}}{\kappa_{r2}}}\lambda_2 r\right)K_0\left(\sqrt{\frac{\kappa_{z2}}{\kappa_{r2}}}\lambda_2 r_2\right)}{K_0\left(\sqrt{\frac{\kappa_{z2}}{\kappa_{r2}}}\lambda_2 r_1\right)I_0\left(\sqrt{\frac{\kappa_{z2}}{\kappa_{r2}}}\lambda_2 r_2\right)-I_0\left(\sqrt{\frac{\kappa_{z2}}{\kappa_{r2}}}\lambda_2 r_1\right)K_0\left(\sqrt{\frac{\kappa_{z2}}{\kappa_{r2}}}\lambda_2 r_2\right)}, \tag{14}$$

where I_0 and K_0 are the modified Bessel functions of the first and second kinds with order zero, respectively. A flowchart to illustrate the procedure for the solution development is shown in Fig. 2.

2.2.1. Development of coefficients a_0 and a_m

The coefficients a_0 and a_m must first be determined. Substituting Eq. (11) into Eq. (8) yields:

$$\tilde{c}_1 a_0+\sum_m a_m\xi_m\cos(\lambda_1 z)=0 \quad \text{for } z_2\leqslant z\leqslant z_1. \tag{15}$$

Putting Eqs. (11) and (12) into Eq. (10) gives:

$$\tilde{c}_1 a_0+\sum_m a_m\xi_m\cos(\lambda_1 z)=\tilde{c}_2(a_0+\Delta h)+\sum_n b_n\eta_n\cos(\lambda_2 z) \quad \text{for } 0\leqslant z\leqslant z_2, \tag{16}$$

where

$$\tilde{c}_1=\frac{\kappa_{r1}}{r_1\ln(r_w/r_1)}, \quad \tilde{c}_2=\frac{\kappa_{r2}}{r_1\ln(r_2/r_1)}, \tag{17}$$

$$\xi_m=\kappa_{r1}\sqrt{\frac{\kappa_{z1}}{\kappa_{r1}}}\lambda_1\tau_1\left(\sqrt{\frac{\kappa_{z1}}{\kappa_{r1}}}\lambda_1 r_1\right), \quad \eta_n=\kappa_{r2}\sqrt{\frac{\kappa_{z2}}{\kappa_{r2}}}\lambda_2\omega_1\left(\sqrt{\frac{\kappa_{z2}}{\kappa_{r2}}}\lambda_2 r_1\right) \tag{18}$$

with

$$\tau_1(\lambda_1 r_1)=\frac{K_1\left(\sqrt{\frac{\kappa_{z1}}{\kappa_{r1}}}\lambda_1 r_1\right)I_0\left(\sqrt{\frac{\kappa_{z1}}{\kappa_{r1}}}\lambda_1 r_w\right)+I_1\left(\sqrt{\frac{\kappa_{z1}}{\kappa_{r1}}}\lambda_1 r_1\right)I_0\left(\sqrt{\frac{\kappa_{z1}}{\kappa_{r1}}}\lambda_1 r_w\right)}{K_0\left(\sqrt{\frac{\kappa_{z1}}{\kappa_{r1}}}\lambda_1 r_1\right)I_0\left(\sqrt{\frac{\kappa_{z1}}{\kappa_{r1}}}\lambda_1 r_w\right)-I_0\left(\sqrt{\frac{\kappa_{z1}}{\kappa_{r1}}}\lambda_1 r_1\right)K_0\left(\sqrt{\frac{\kappa_{z1}}{\kappa_{r1}}}\lambda_1 r_w\right)}, \tag{19}$$

$$\omega_1(\lambda_2 r_1)=\frac{K_1\left(\sqrt{\frac{\kappa_{z2}}{\kappa_{r2}}}\lambda_2 r_1\right)I_0\left(\sqrt{\frac{\kappa_{z2}}{\kappa_{r2}}}\lambda_2 r_2\right)+I_1\left(\sqrt{\frac{\kappa_{z2}}{\kappa_{r2}}}\lambda_2 r_1\right)K_0\left(\sqrt{\frac{\kappa_{z2}}{\kappa_{r2}}}\lambda_2 r_2\right)}{K_0\left(\sqrt{\frac{\kappa_{z2}}{\kappa_{r2}}}\lambda_2 r_1\right)I_0\left(\sqrt{\frac{\kappa_{z2}}{\kappa_{r2}}}\lambda_2 r_2\right)-I_0\left(\sqrt{\frac{\kappa_{z2}}{\kappa_{r2}}}\lambda_2 r_1\right)K_0\left(\sqrt{\frac{\kappa_{z2}}{\kappa_{r2}}}\lambda_2 r_2\right)}, \tag{20}$$

where I_1 and K_1 are the modified Bessel functions of the first and second kinds with order one, respectively.

The procedure in determining a_0 and a_m in Eqs. (15) and (16) is given in Appendix B and the results are

$$a_0=\frac{1}{\tilde{c}_1 z_1/\tilde{c}_2 z_2-1}\Delta h \tag{21}$$

and

$$a_j\xi_j=\Gamma_j(a_0+\Delta h)+\sum_n \Theta_{jn}\eta_n b_n, \tag{22}$$

where $j = 1,2,3,\ldots$, $a_j = a_m$, and

$$\Gamma_j = \frac{2\tilde{c}_2}{\lambda_1 z_1}\sin(\lambda_1 z_2), \tag{23}$$

$$\Theta_{jn} = \frac{\sin(\lambda_2 z_2 + \lambda_1 z_2)}{\lambda_2 z_1 + \lambda_1 z_1} + \frac{\sin(\lambda_2 z_2 - \lambda_1 z_2)}{\lambda_2 z_1 - \lambda_1 z_1} \quad \text{for } \lambda_1 \neq \lambda_2, \tag{24}$$

$$\Theta_{jn} = \frac{z_2}{z_1} \quad \text{for } \lambda_1 = \lambda_2. \tag{25}$$

2.2.2. Development of coefficients b_n

Substituting Eqs. (11) and (12) into Eq. (9) leads to

$$\sum_m a_m \tau_0\left(\sqrt{\frac{\kappa_{z1}}{\kappa_{r1}}}\lambda_1 r_1\right)\cos(\lambda_1 z) = \sum_n b_n \omega_0\left(\sqrt{\frac{\kappa_{z2}}{\kappa_{r2}}}\lambda_2 r_1\right)\cos(\lambda_2 z) \quad \text{for } 0 \leqslant z \leqslant z_2. \tag{26}$$

According to Eqs. (13) and (14), at $r = r_1$, one can obtain

$$\tau_0\left(\sqrt{\frac{\kappa_{z1}}{\kappa_{r1}}}\lambda_1 r_1\right) = 1, \quad \omega_0\left(\sqrt{\frac{\kappa_{z2}}{\kappa_{r2}}}\lambda_2 r_1\right) = 1. \tag{27}$$

Eq. (26) can be simplified as

$$\sum_m a_m \cos(\lambda_1 z) = \sum_n b_n \cos(\lambda_2 z) \quad \text{for } 0 \leqslant z \leqslant z_2. \tag{28}$$

The development of coefficients b_n is shown in Appendix C and the result is

$$b_n = \sum_m \Lambda_{nm} a_m, \tag{29}$$

where

$$\Lambda_{nm} = \frac{\sin(\lambda_1 z_2 + \lambda_2 z_2)}{\lambda_1 z_2 + \lambda_2 z_2} + \frac{\sin(\lambda_1 z_2 - \lambda_2 z_2)}{\lambda_1 z_2 - \lambda_2 z_2} \quad \text{for } \lambda_1 \neq \lambda_2, \tag{30}$$

$$\Lambda_{nm} = 1 \quad \text{for } \lambda_1 = \lambda_2. \tag{31}$$

2.2.3. Determination of coefficients a_m and b_n

The analytical expressions for hydraulic head distributions in Eqs. (11) and (12) can be obtained after determining the coefficients a_m and b_n given in Eqs. (22) and (29). One can insert Eqs. (21) and (29) into (22) and obtain the following linear equations

$$\sum_m (\beta_{jm} - \xi_j) a_m = \alpha_j \Delta h, \tag{32}$$

where ξ_j defined in Eq. (18) is equal to zero when $j \neq m$, and

$$\alpha_j = \frac{1}{\tilde{c}_2 z_2/\tilde{c}_1 z_1 - 1}\Gamma_j, \tag{33}$$

$$\beta_{jm} = \sum_n \Theta_{jn}\eta_n \Lambda_{nm}. \tag{34}$$

The constants a_m in Eq. (32) can be determined by solving the system of equations. The coefficient of b_n can then be obtained from Eq. (29).

The solution describing the steady-state head distribution for flow injection to the anticline reservoir with heterogeneous and anisotropic conductivity is mainly composed of Eqs. (11), (12), (21), (22), (29) and (32). In addition, these equations can be simplified for the case of a homogeneous and isotropic reservoir if one sets $\kappa_{r1} = \kappa_{z1} = \kappa_{r2} = \kappa_{z2}$ and $z_1 = z_2$ for the flat reservoir.

2.3. Injection rate

The volumetric flow rate due to injection at the wellbore can be estimated by integrating the hydraulic head gradient along the rim of the wellbore as

$$Q_w = \int_0^{z_1} 2\pi\kappa_{r1} r_w \left.\frac{\partial h_1}{\partial r}\right|_{r=r_w} dz. \tag{35}$$

According to Eq. (11), one can write

$$\left.\frac{\partial h_1}{\partial r}\right|_{r=r_w} = \frac{a_0}{r_w \ln(r_w/r_1)} + \sum_m a_m \lambda_1 \sqrt{\frac{\kappa_{z1}}{\kappa_{r1}}}\tau_1\left(\sqrt{\frac{\kappa_{z1}}{\kappa_{r1}}}\lambda_1 r_w\right)\cos(\lambda_1 z). \tag{36}$$

Substituting Eq. (36) into Eq. (35) yields

$$Q_w = \frac{2\pi\kappa_{r1} z_1}{\ln(r_w/r_1)} a_0. \tag{37}$$

With Eqs. (17) and (21), Eq. (37) can be presented as

$$Q_w = \frac{2\pi\kappa_{r1}\kappa_{r2} z_1 z_2}{\kappa_{r1} z_1 \ln(r_2/r_1) - \kappa_{r2} z_2 \ln(r_w/r_1)}\Delta h. \tag{38}$$

Eq. (38) indicates that the injection flow rate depends on r_2 which is defined as the distance from the center of the well to the outer boundary. Mathematically, a constant-head condition can be specified at the outer boundary if a water body is present there. As such, r_2 can be measured from the field. Otherwise, r_2 is considered as the influence radius (or radius of influence) which represents the distance from the center of the well to the edge of the cone of depression. Therefore, the drawdown is zero at the outer boundary. Bear [13] mentioned three semi-empirical and two empirical formulas for determining r_2. For the semi-empirical formulas, r_2 depends on the time or precipitation and are thus not applicable to Eq. (38). On the other hand, those two empirical formulas relating hydraulic conductivity to aquifer drawdown (or buildup for injection) can be employed to estimate r_2. Since r_2 is in the form of $\ln r_2$, a large error produced when estimating r_2 may not significantly affect the injection rate estimated by Eq. (38) [14].

2.4. Special cases: homogeneous and isotropic anticline, two conductivity zones, and Thiem equation

When the reservoir is a homogeneous and isotropic anticline, i.e., $\kappa_h = \kappa_{r1} = \kappa_{z1} = \kappa_{r2} = \kappa_{z2}$, Eq. (38) can be reduced to

$$Q_h = \frac{2\pi\kappa_h z_2}{\ln(r_2/r_1) - (z_2/z_1)\ln(r_w/r_1)}\Delta h. \tag{39}$$

Consider an isotropic reservoir with two concentric conductivity zones being flat (the thickness of the reservoir is uniform, i.e., $z_f = z_1 = z_2$) and the first zone of the reservoir may be taken as a skin (i.e., $\kappa_{r1} \neq \kappa_{r2}$) [15,16]. Eq. (38) can be simplified as

$$Q_f = \frac{2\pi\kappa_{r2} z_f}{\ln(r_2/r_1) - (\kappa_{r2}/\kappa_{r1})\ln(r_w/r_1)}\Delta h. \tag{40}$$

Furthermore, if the reservoir is homogeneous and flat, then Eq. (40) becomes

$$Q_o = \frac{2\pi\kappa_h z_f}{\ln(r_2/r_w)}\Delta h \tag{41}$$

which is indeed the Thiem equation.

3. Results and discussion

For demonstration, a case where fluid is injected into an anticline reservoir through a fully penetrating well with $r_w = 0.2$ m is assumed. The thicknesses of regions 1 and 2 (i.e., z_1 and z_2) of the reservoir are respectively assumed to be 30 m and 20 m which are commonly seen in western Taiwan [2]. The distance from the center of the injection well to the interface between both regions and the outer boundary (i.e., r_1 and r_2) are 10 m and 500 m, respectively. For this homogeneous and isotropic reservoir, the hydraulic conductivities in regions 1 and 2 are assumed to be 1 m/day. The hydraulic heads at the wellbore and the outer boundary (i.e., h_w

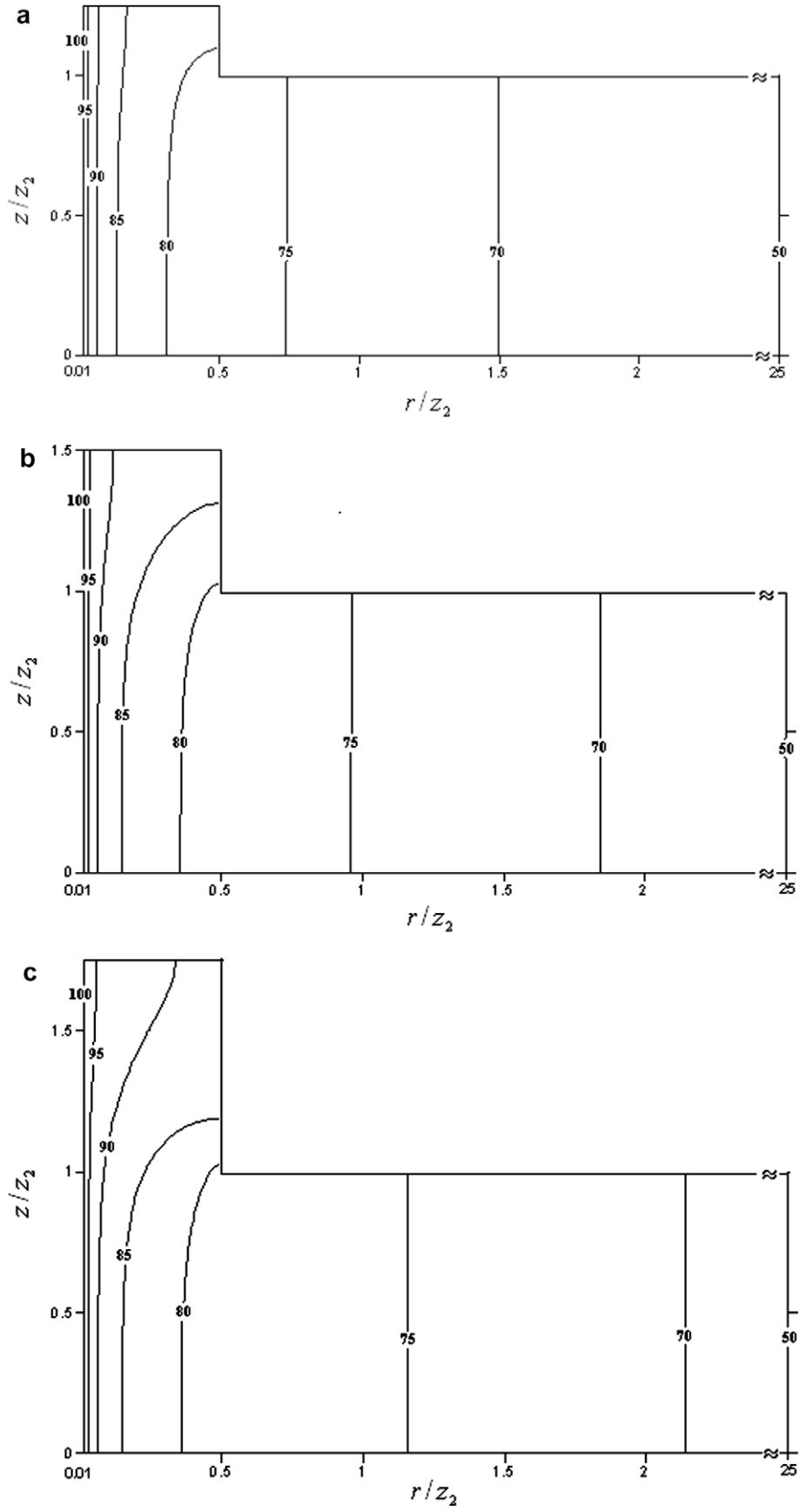

Fig. 3. Hydraulic head distribution in a homogeneous and isotropic formation for $r_1/z_2 = 0.5,\ r_2/z_2 = 25,\ \Delta h = 50$ m with z_δ/z_2 (a) 0.25, (b) 0.5, and (c) 0.75.

and h_o) are 100 m and 50 m, respectively. That is $\Delta h = 50$ m which is equivalent to a pressure of 9.36 MPa when considering injection of CO_2 under normal conditions [17]. The present solution is used for investigating the effects of reservoir geometry as well as heterogeneity and anisotropic on the head distribution in anticline formations.

3.1. Effects of trap height and width on hydraulic head distribution

To investigate the influence of anticline trapping geometry on the flow field, various values of the dimensionless trap height (z_δ/z_2) and trap width (r_1/z_2) are taken to simulate shallow and deep traps of a homogeneous reservoir. Fig. 3(a)–(c) shows the contour lines of the hydraulic head for the reservoir with $r_1/z_2 = 0.5$, $r_2/z_2 = 25$, and $\Delta h = 50$ m when the dimensionless trap heights are 0.25, 0.5, and 0.75, respectively. These figures indicate that the head drops quickly inside the trap for the case of a reservoir with a large trap height. In contrast, a reservoir with a small trap height will cause a mild head drop in the first zone.

The effect of trap width on the head distribution for reservoir with a dimensionless trap height of 0.5 is shown in Figs. 3(b), 4(a), and (b). These figures indicate that the reservoir with a small dimensionless trap width (say, 0.25) introduces higher hydraulic head within the trap than those with larger dimensionless trap widths such as $r_1/z_2 = 0.5$ and 0.75.

Note that the trap areas are the same for the reservoirs shown in Figs. 3(c) and 4(b). The trap in Fig. 3(c) has a dimension of 10 m (width) $\times$ 15 m (height) while that in Fig. 4(b) has a dimension of 15 m $\times$ 10 m. Comparing Fig. 3(c) with Fig. 4(b) for the head distribution reveals that the hydraulic head shown in Fig. 3(c) is significantly higher than that in Fig. 4(b). In other words, a steeply folded anticline will introduce a higher head distribution than a gently folded one if the areas of the trap in the anticlines are the same for a constant head injection.

3.2. Effect of outer boundary on hydraulic head distribution

For a fixed trap geometry and constant Δh, the effect of outer boundary (in terms of r_2/z_2) on the hydraulic head distribution is

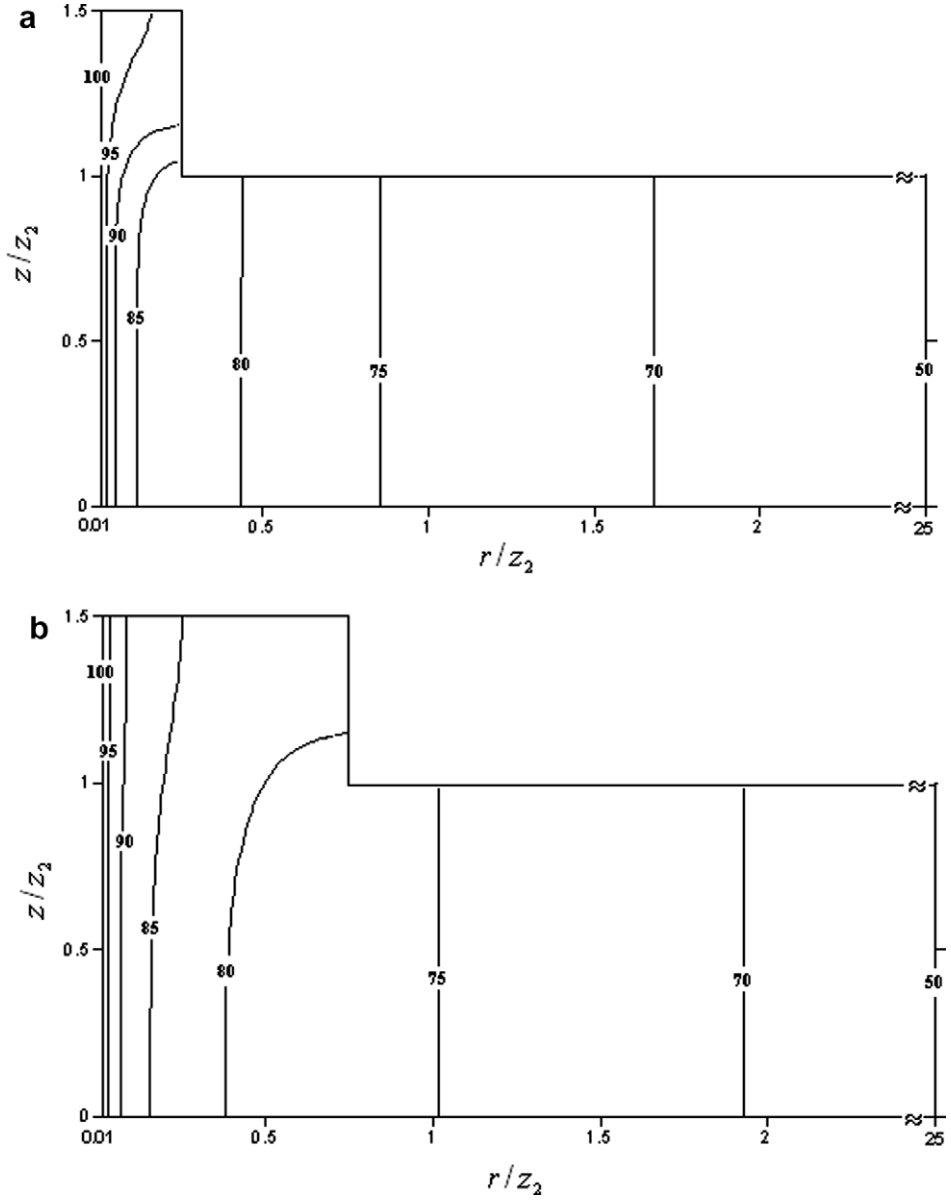

Fig. 4. Hydraulic head distribution in a homogeneous and isotropic formation for $z_\delta/z_2 = 0.5$, $r_2/z_2 = 25$, $\Delta h = 50$ m with r_1/z_2 (a) 0.25 and (b) 0.75.

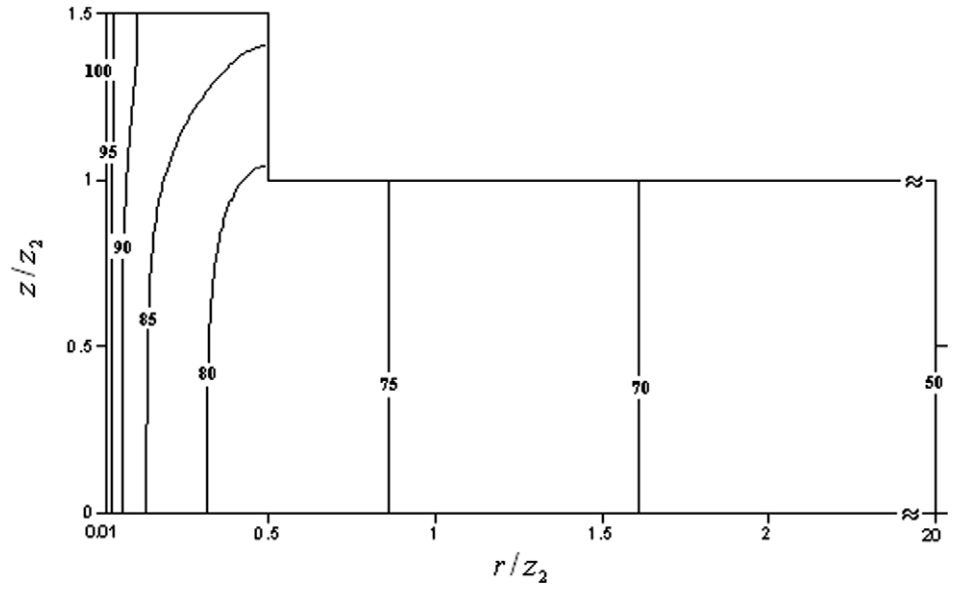

Fig. 5. Hydraulic head distribution in a homogeneous and isotropic formation for $z_\delta/z_2 = 0.5,\ r_1/z_2 = 0.5$, and $\Delta h = 50$ m when $r_2/z_2 = 20$.

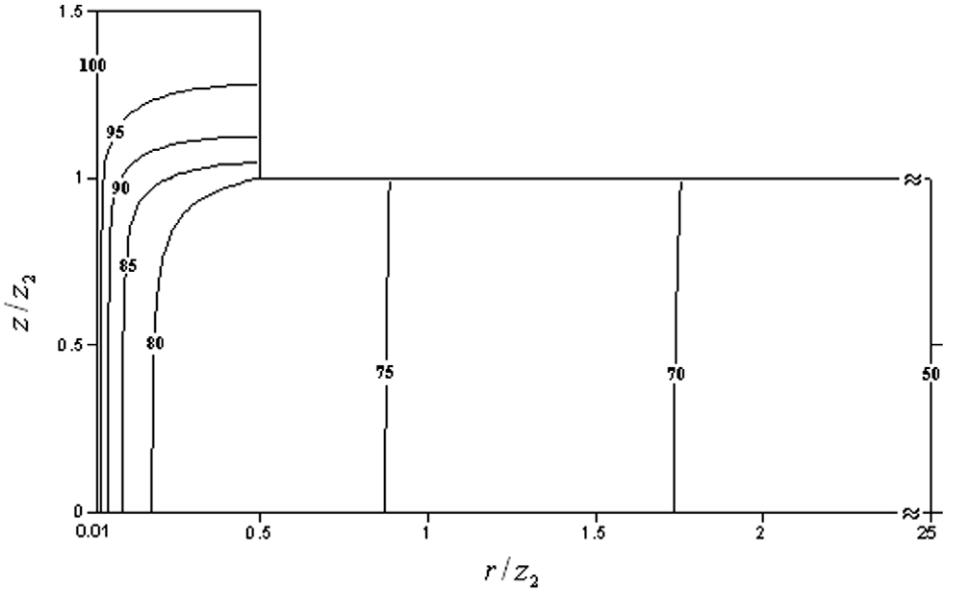

Fig. 6. Hydraulic head distribution in a homogeneous but anisotropic formation with $\kappa_{r1}/\kappa_{r2} = 10$ for $z_\delta/z_2 = 0.5,\ r_1/z_2 = 0.5,\ r_2/z_2 = 25$, and $\Delta h = 50$ m.

studied herein. Fig. 5 exhibits the hydraulic head distribution for $r_2/z_2 = 20$ with $z_\delta/z_2 = 0.5$ and $r_1/z_2 = 0.5$. The influence of the outer boundary (r_2/z_2) on the head distribution is insignificant, especially in region 1 when comparing the contour distribution in Fig. 5 with that in Fig. 3(b), where $r_2/z_2 = 25$.

3.3. Effect of anisotropy on head distribution

The effect of anisotropy on head distribution in a homogeneous formation (i.e., $\kappa_{r1} = \kappa_{r2}$ and $\kappa_{z1} = \kappa_{z2}$) is investigated herein. Fig. 6 demonstrates the head distribution of the anisotropic anticline reservoir with $\kappa_{r1}/\kappa_{z1} = 10$. As seen when comparing Fig. 6 with 3(b), high-pressure gradients and vertical flow in the upper part of the trap are apparent because of the small vertical conductivity.

3.4. Effect of heterogeneity on head distribution

This section is to examine the effect of heterogeneity on the head distribution in an isotropic formation (i.e., $\kappa_{r1} = \kappa_{z1}$ and $\kappa_{r2} = \kappa_{z2}$). The head distributions for reservoirs with uniform thickness $(z_\delta = 0)$ but different conductivity ratios, such as $\kappa_{r1}/\kappa_{r2} = 0.5$, 1 and 2, are plotted in Fig. 7(a)–(c), respectively. Region 1 has a lower conductivity than region 2 if $\kappa_{r1}/\kappa_{r2} = 0.5$ and a higher conductivity than region 2 if $\kappa_{r1}/\kappa_{r2} = 2$. These figures indicate that when the conductivity of region 1 is smaller than that of region 2, region 1 has a denser head contour. In other words, the head in region 1 drops rapidly for a smaller κ_{r1}/κ_{r2}. On the other hand, the head change in region 1, which has a higher conductivity, in Fig. 7(c) is relatively smaller than those in Fig. 7(a) and (b).

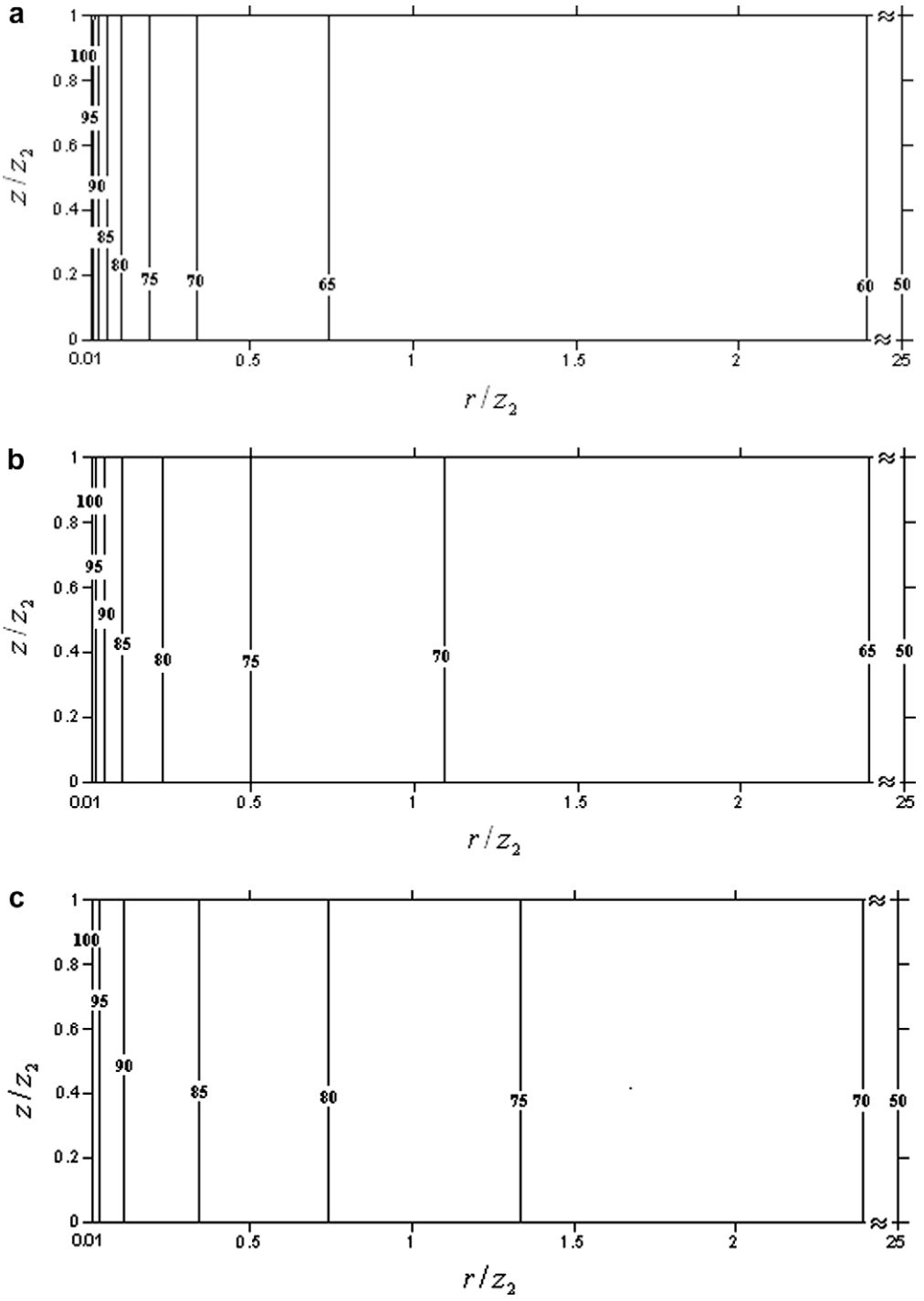

Fig. 7. Hydraulic head distribution in an isotropic but heterogeneous formation with κ_{r1}/κ_{r2} (a) 0.5, (b) 1, and (c) 2 for $z_\delta/z_2 = 0,\ r_1/z_2 = 0.5,\ r_2/z_2 = 25$, and $\Delta h = 50$ m.

3.5. Effects of trap shape and area on injection rate

The injection rate for a homogeneous, isotropic and flat reservoir system, Q_o, can be determined from Eq. (41). On the other hand, the injection rate for an anticline reservoir, Q_h, can be obtained from Eq. (39). The injection rate with conditions given at the beginning of Section 3 obtained from Eq. (41) is $Q_o = 803.06\ \mathrm{m}^3/\mathrm{day}$. Then the curves for Q_h/Q_o (dimensionless injection rate) versus z_δ/r_1 (ratio of trap height over width) can be employed to assess the impact of trap shape and areas on injection rate.

The dashed line of Fig. 8 shows that Q_h/Q_o increases with z_δ/r_1 when $r_1/z_2 = 0.5$. This indicates that a taller trap has a higher injection rate for a fixed trap width. In contrast, the solid line displays that Q_h/Q_o is inversely proportional to z_δ/r_1 when $z_\delta/z_2 = 0.5$. In other words, the proportion of Q_h to r_1 implies that a wider trap yields a higher injection rate for a fixed trap height. Fig. 8 also shows that the solid line intersects the dashed line at $z_\delta/r_1 = 1$ and $Q_h/Q_o = 1.2$. For a fixed trap width, a taller trap will have a larger trap area. On the other hand, a wider trap also has a larger trap area for a fixed trap height. Obviously, a larger trap area causes a higher injection rate.

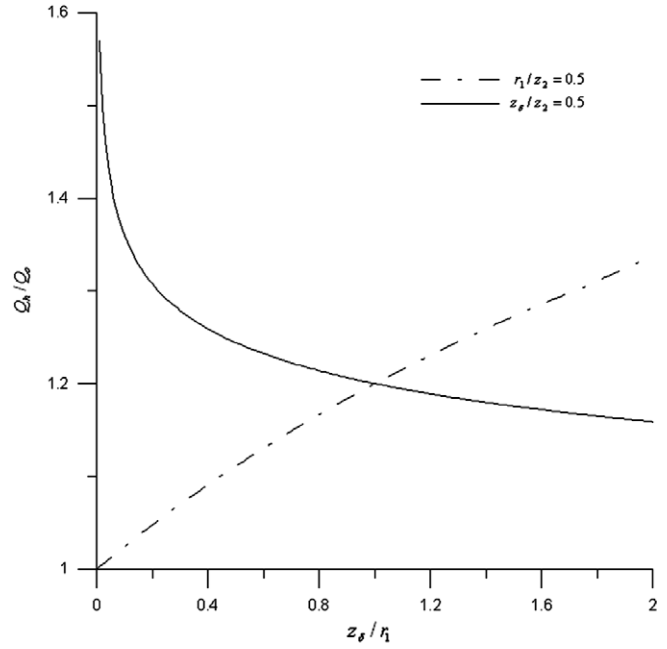

Fig. 8. Dimensionless injection rate versus trap shape with $r_1/z_2 = 0.5$ and $z_\delta/z_2 = 0.5$ for $r_2/z_2 = 25$ and $\Delta h = 50$ m when considering $\kappa_h = \kappa_{r1} = \kappa_{z1} = \kappa_{r2} = \kappa_{z2}$.

Additionally, one can get $Q_h/Q_o = 1.25$ for z_δ/r_1 at 0.46 from the solid line (i.e., gently folded anticlines) or 1.33 from the dashed line (i.e., steeply folded anticlines) in Fig. 8. The trap area is 217.39 m^2 for the former and 133 m^2 for the latter. It is interesting to note that different trap areas get the same injection rate. Obviously, a steeply folded anticline can have the same injection rate as a gently folded one even when the trap area of the steeply folded anticline is smaller than that of the gently folded one.

4. Conclusions

A new analytical solution has been developed for simulating the head distribution after fluid injection into a heterogeneous and anisotropic anticline reservoir. This solution can be employed to estimate volumetric flow rates of a flat reservoir with two concentric transmissivity zones. One can further use this solution to assess the skin effect on the head distribution if the reservoir is flat and the first zone of the heterogeneous reservoir represents the well skin. In addition, the equation developed for determining the injection rate can be reduced to the Thiem equation if the reservoir is flat, homogeneous and isotropic.

The effects of changes in trap height and width on head distribution in the anticline formation are investigated. The results show that the head within the trap increases with trap height and decreases with increasing trap width. Moreover, the impacts of formation heterogeneity and anisotropy on the head distribution are also assessed. The results indicate that when the conductivity of the first region is smaller than that of the second region, then the first region has a higher head distribution than the second one. On the other hand, the first region with a higher conductivity will introduce lower head distribution than the second one. A taller trap results in a higher injection rate for a fixed trap width; on the other hand, a wider trap causes a higher injection rate for a fixed trap height. In other words, a larger trap area generally results in a higher injection rate. However, a steeply folded anticline can have the same injection rate as a gently folded one even when the trap area of the steeply folded anticline is smaller than that of the gently folded one. These results demonstrate that the present solution can be used as a preliminary tool to assess the strategies of long-term fluid injection, liquid waste sequestration, or other similar engineering practices to anticline reservoirs.

Acknowledgements

Research leading to this work has been partially supported by the Grants from Taiwan National Science Council under the contract number NSC 96-2221-E-009-087-MY3. The authors would like to thank three anonymous reviewers for their valuable and constructive comments that help improve the clarity of our presentation.

Appendix A. Development of Eqs. (11) and (12)

The solution describing the hydraulic head distribution in regions 1 and 2 is developed in this appendix.

A.1. Region 1

One can solve Eq. (1) with Eqs. (3) and (4) using the method of separation of variables. The result is

$$h_1 = E_0 + F_0 \ln r + \sum_m \left[E_m I_0\left(\sqrt{\frac{\kappa_{z1}}{\kappa_{r1}}}\lambda_1 r\right) + F_m K_0\left(\sqrt{\frac{\kappa_{z1}}{\kappa_{r1}}}\lambda_1 r\right)\right]\cos(\lambda_1 z), \tag{A1}$$

where E_0, F_0, E_m and F_m are constants and should be determined. At $r = r_w$, with Eqs. (A1) and (2), we get

$$h_w = E_0 + F_0 \ln r_w + \sum_m \left[E_m I_0\left(\sqrt{\frac{\kappa_{z1}}{\kappa_{r1}}}\lambda_1 r_w\right) + F_m K_0\left(\sqrt{\frac{\kappa_{z1}}{\kappa_{r1}}}\lambda_1 r_w\right)\right]\cos(\lambda_1 z). \tag{A2}$$

Since E_0, F_0, r_w, and h_w are all independent on z, the bracket term in Eq. (A2) has to be zero. That is

$$E_m I_0\left(\sqrt{\frac{\kappa_{z1}}{\kappa_{r1}}}\lambda_1 r_w\right) + F_m K_0\left(\sqrt{\frac{\kappa_{z1}}{\kappa_{r1}}}\lambda_1 r_w\right) = 0. \tag{A3}$$

Thus, one can obtain

$$h_w = E_0 + F_0 \ln r_w. \tag{A4}$$

From Eq. (A1), the hydraulic head $\Psi(z)$ at $r = r_1$ can be expressed as

$$\Psi(z) = E_0 + F_0 \ln r_1 + \sum_m \left[E_m I_0\left(\sqrt{\frac{\kappa_{z1}}{\kappa_{r1}}}\lambda_1 r_1\right) + F_m K_0\left(\sqrt{\frac{\kappa_{z1}}{\kappa_{r1}}}\lambda_1 r_1\right)\right]\cos(\lambda_1 z). \tag{A5}$$

The average hydraulic head, H, over the thickness of z_1 obtained from Eq. (A5) is

$$H = \frac{1}{z_1}\int_0^{z_1} \Psi(z)dz = E_0 + F_0 \ln r_1. \tag{A6}$$

The bracket term in Eq. (A5) is defined as an unknown constant, a_m

$$a_m = -\left[E_m I_0\left(\sqrt{\frac{\kappa_{z1}}{\kappa_{r1}}}\lambda_1 r_1\right) + F_m K_0\left(\sqrt{\frac{\kappa_{z1}}{\kappa_{r1}}}\lambda_1 r_1\right)\right]. \tag{A7}$$

From Eqs. (A4) and (A6), one can obtain

$$E_0 = h_w - (H - h_w)\frac{\ln r_w}{\ln(r_1/r_w)} \tag{A8}$$

and

$$F_0 = \frac{H - h_w}{\ln(r_1/r_w)}. \tag{A9}$$

With Eqs. (A3) and (A7), one can solve for the constants E_m and F_m. The results are

$$E_m = \frac{a_m K_0\left(\sqrt{\frac{\kappa_{z1}}{\kappa_{r1}}}\lambda_1 r_w\right)}{K_0\left(\sqrt{\frac{\kappa_{z1}}{\kappa_{r1}}}\lambda_1 r_1\right) I_0\left(\sqrt{\frac{\kappa_{z1}}{\kappa_{r1}}}\lambda_1 r_w\right) - I_0\left(\sqrt{\frac{\kappa_{z1}}{\kappa_{r1}}}\lambda_1 r_1\right) K_0\left(\sqrt{\frac{\kappa_{z1}}{\kappa_{r1}}}\lambda_1 r_w\right)} \tag{A10}$$

and

$$F_m = \frac{-a_m I_0\left(\sqrt{\frac{\kappa_{z1}}{\kappa_{r1}}}\lambda_1 r_w\right)}{K_0\left(\sqrt{\frac{\kappa_{z1}}{\kappa_{r1}}}\lambda_1 r_1\right) I_0\left(\sqrt{\frac{\kappa_{z1}}{\kappa_{r1}}}\lambda_1 r_w\right) - I_0\left(\sqrt{\frac{\kappa_{z1}}{\kappa_{r1}}}\lambda_1 r_1\right) K_0\left(\sqrt{\frac{\kappa_{z1}}{\kappa_{r1}}}\lambda_1 r_w\right)}. \tag{A11}$$

Substituting Eqs. (A8)–(A11) into Eq. (A1) results in Eq. (11).

A.2. Region 2

Similar to the development for Eq. (A1) given above, substituting Eqs. (6) and (7) into Eq. (1) results in

$$h_2 = \overline{E}_0 + \overline{F}_0 \ln r + \sum_n \left[E_n I_0\left(\sqrt{\frac{\kappa_{z2}}{\kappa_{r2}}}\lambda_2 r\right) + F_n K_0\left(\sqrt{\frac{\kappa_{z2}}{\kappa_{r2}}}\lambda_2 r\right)\right]\cos(\lambda_2 z), \tag{A12}$$

where $\overline{E}_0$, $\overline{F}_0$, E_n and F_n are also unknown constants.

At $r = r_2$, the result after substituting Eq. (5) into Eq. (A12) is

$$h_o = \overline{E}_0 + \overline{F}_0 \ln r_2 + \sum_n \left[E_n I_0\left(\sqrt{\frac{\kappa_{z2}}{\kappa_{r2}}}\lambda_2 r_2\right) + F_n K_0\left(\sqrt{\frac{\kappa_{z2}}{\kappa_{r2}}}\lambda_2 r_2\right)\right]\cos(\lambda_2 z). \tag{A13}$$

Because $\overline{E}_0$, $\overline{F}_0$, h_o, and r_2 are not function of z, the bracket term in Eq. (A13) has to be zero. In other words,

$$E_n I_0\left(\sqrt{\frac{\kappa_{z2}}{\kappa_{r2}}}\lambda_2 r_2\right) + F_n K_0\left(\sqrt{\frac{\kappa_{z2}}{\kappa_{r2}}}\lambda_2 r_2\right) = 0. \tag{A14}$$

Thus, one can get

$$h_o = \overline{E}_0 + \overline{F}_0 \ln r_2. \tag{A15}$$

The hydraulic head $\Psi(z)$ at $r = r_1$ defined by Eqs. (A12) and (9) is

$$\Psi(z) = \overline{E}_0 + \overline{F}_0 \ln r_1 + \sum_n \left[E_n I_0\left(\sqrt{\frac{\kappa_{z2}}{\kappa_{r2}}}\lambda_2 r_1\right) + F_n K_0\left(\sqrt{\frac{\kappa_{z2}}{\kappa_{r2}}}\lambda_2 r_1\right)\right]\cos(\lambda_2 z). \tag{A16}$$

The average hydraulic head at the interface between regions 1 and 2 can be obtained from Eq. (A16) as

$$H = \frac{1}{z_1}\int_0^{z_1} \Psi(z)dz = \overline{E}_0 + \overline{F}_0 \ln r_1. \tag{A17}$$

Assume that

$$b_n = -\left[E_n I_0\left(\sqrt{\frac{\kappa_{z2}}{\kappa_{r2}}}\lambda_2 r_1\right) + F_n K_0\left(\sqrt{\frac{\kappa_{z2}}{\kappa_{r2}}}\lambda_2 r_1\right)\right]. \tag{A18}$$

The constant $\overline{E}_0$ and $\overline{F}_0$ obtained from Eqs. (A15) and (A17) are

$$\overline{E}_0 = h_o - (H - h_o)\frac{\ln r_2}{\ln(r_1/r_2)} \tag{A19}$$

and

$$\overline{F}_0 = \frac{H - h_o}{\ln(r_1/r_2)}. \tag{A20}$$

With Eqs. (A14) and (A18), the constants E_n and F_n can then be solved as

$$E_n = \frac{b_n K_0\left(\sqrt{\frac{\kappa_{z2}}{\kappa_{r2}}}\lambda_2 r_2\right)}{K_0\left(\sqrt{\frac{\kappa_{z2}}{\kappa_{r2}}}\lambda_2 r_1\right) I_0\left(\sqrt{\frac{\kappa_{z2}}{\kappa_{r2}}}\lambda_2 r_2\right) - I_0\left(\sqrt{\frac{\kappa_{z2}}{\kappa_{r2}}}\lambda_2 r_1\right) K_0\left(\sqrt{\frac{\kappa_{z2}}{\kappa_{r2}}}\lambda_2 r_2\right)} \tag{A21}$$

and

$$F_n = \frac{-b_n I_0\left(\sqrt{\frac{\kappa_{z2}}{\kappa_{r2}}}\lambda_2 r_2\right)}{K_0\left(\sqrt{\frac{\kappa_{z2}}{\kappa_{r2}}}\lambda_2 r_1\right) I_0\left(\sqrt{\frac{\kappa_{z2}}{\kappa_{r2}}}\lambda_2 r_2\right) - I_0\left(\sqrt{\frac{\kappa_{z2}}{\kappa_{r2}}}\lambda_2 r_1\right) K_0\left(\sqrt{\frac{\kappa_{z2}}{\kappa_{r2}}}\lambda_2 r_2\right)}. \tag{A22}$$

Substituting Eqs. (A19) to (A22) into Eq. (A12) results in Eq. (12).

Appendix B. Development of a_0 and a_m

Integrating the right-hand side (RHS) of Eq. (16) from 0 to z_2 and the RHS of Eq. (15) from z_2 to z_1, the sum of the integration results is further divided by z_1 to determine $\tilde{c}_1 a_0$

$$\tilde{c}_1 a_0 = \frac{\int_0^{z_2}\left[\tilde{c}_2(a_0 + \Delta h) + \sum_n b_n \eta_n \cos(\lambda_2 z)\right]dz}{z_1}. \tag{B1}$$

Integrating Eq. (B1) leads to Eq. (21).

For the determination of $a_m \xi_m$, both Eqs. (15) and (16) are first multiplied by $2\cos(\lambda_1 z)$. Then one can integrate the RHS of Eq. (16) from 0 to z_2 and the RHS of Eq. (15) from z_2 to z_1. Summing up the integrations and then dividing the result by z_1 gives

$$a_m \xi_m = \frac{2\int_0^{z_2}\left[\tilde{c}_2(a_0 + \Delta h) + \sum_n b_n \eta_n \cos(\lambda_2 z)\right]\cos(\lambda_1 z)dz}{z_1}. \tag{B2}$$

The numerator terms in Eq. (B2) can be expressed respectively as

$$2\int_0^{z_2} \tilde{c}_2(a_0 + \Delta h)\cos(\lambda_1 z)dz = 2\frac{\tilde{c}_2}{\lambda_1}(a_0 + \Delta h)\sin(\lambda_1 z_2) \tag{B3}$$

$$2\int_0^{z_2} \sum_n b_n \eta_n \cos(\lambda_2 z)\cos(\lambda_1 z)dz = \int_0^{z_2} \sum_n b_n \eta_n [\cos(\lambda_2 z + \lambda_1 z) + \cos(\lambda_2 z - \lambda_1 z)]dz. \tag{B4}$$

The RHS of (B4) reduces to

$$\sum_n b_n \eta_n \left[\frac{\sin(\lambda_2 z_2 + \lambda_1 z_2)}{\lambda_2 + \lambda_1} + \frac{\sin(\lambda_2 z_2 - \lambda_1 z_2)}{\lambda_2 - \lambda_1}\right] \tag{B5}$$

if $\lambda_1 \neq \lambda_2$; otherwise, it turns into

$$z_2 \sum_n b_n \eta_n. \tag{B6}$$

Substituting Eqs. (B3), (B5) and (B6) into (B2) results in

$$a_m \xi_m = \Gamma_m(a_0 + \Delta h) + \sum_n \Theta_{mn} \eta_n b_n. \tag{B7}$$

Finally, Eq. (22) can be obtained when the subscript m in Eq. (B7) is replaced by j to avoid confusing with the one in Eq. (29).

Appendix C. Development of b_n

The constant b_n can be determined from integrating the RHS of Eq. (26) multiplied by $2\cos(\lambda_2 z)$ from 0 to z_2 and dividing it by z_2 as

$$b_n = \frac{2\int_0^{z_2} \sum_m a_m \cos(\lambda_1 z)\cos(\lambda_2 z)dz}{z_2}. \tag{C1}$$

Performing the integration of the numerator in Eq. (C1) over z results in

$$2\int_0^{z_2}\sum_m a_m\cos(\lambda_1 z)\cos(\lambda_2 z)dz = \int_0^{z_2}\sum_n a_m[\cos(\lambda_1 z+\lambda_2 z)+\cos(\lambda_1 z-\lambda_2 z)]dz. \quad (C2)$$

The RHS of Eq. (C2) becomes

$$\sum_m a_m\left[\frac{\sin(\lambda_1 z_2+\lambda_2 z_2)}{\lambda_1+\lambda_2}+\frac{\sin(\lambda_1 z_2-\lambda_2 z_2)}{\lambda_1-\lambda_2}\right] \quad (C3)$$

when $\lambda_1 \neq \lambda_2$; otherwise it reduces to

$$z_2\sum_m a_m. \quad (C4)$$

Finally, one can obtain (29) after substituting Eqs. (C3) and (C4) into (C1).

References

[1] Bear J. Dynamics of fluids in porous media. New York: American Elsevier Publishing Company Inc.; 1972.
[2] Lai TC, Fei LY, Chiang CJ. The characteristics of groundwater zones in Taiwan, Hydrogeological survey and application workshop, Taiwan, 2003. p. 1–24.
[3] Fuh SC, Liang SC. Miocene Talu sand pinch out study and its application to hydrocarbon potential assessment, Western Onshore and Offshore Taiwan. J Petrol 2006;42(2):1–18.
[4] Al-Mohannadi N, Ozkan E, Kazemi H. Pressure-transient responses of horizontal and curved wells in anticlines and domes. SPEREE 2007:66–76.
[5] Saripalli KP, Sharma MM, Bryant SL. Modeling injection well performance during deep-well injection of liquid wastes. J Hydrol 2000;227:41–55.
[6] Natoli VD, Pergler J, Mifflin R. Ewald method for the analytic solution of simple reservoir problems with Neumann boundary conditions. SPE J 2004:122–7.
[7] Boughrara AA, Peres AMM, Chen S, Machado AAV, Reynolds AC. Approximate analytical solutions for the pressure response at a water-injection well. SPE J 2007:19–34.
[8] Kirkham D. Exact theory of flow into a partially penetrating well. J Geophys Res 1959;64(9):1317–27.
[9] Javandel I, Zaghim N. Analysis of flow to an extended fully penetrating well. Water Resour Res 1975;11(1):159–64.
[10] Spiegel MR. Schaum's outline of theory and problems of fourier analysis; with applications to boundary value problems. New York: McGraw-Hill Book Company, Inc.; 1974.
[11] Chen CS. A reinvestigation of the analytical solution for drawdown distributions in a finite confined aquifer. Water Resour Res 1984;20(10):1466–8.
[12] Wang CT, Yeh HD. Obtaining the steady-state drawdown solutions of constant-head and constant-flux tests. Hydrol Process 2008;22(17):3456–61. doi:10.1002/hyp.6950.
[13] Bear J. Hydraulics of groundwater. New York: McGraw-Hill Inc.; 1979.
[14] Batu V. Aquifer hydraulics. New York: John Wiley & Sons; 1998.
[15] Yeh HD, Yang SY. A novel analytical solution for a slug test conducted in a well with a finite-thickness skin. Adv Water Resour 2006;29(10):1479–89. doi:10.1016/j.advwatres.2005.11.002.
[16] Yeh HD, Chen YJ. Determination of skin and aquifer parameters for a slug test with wellbore-skin effect. J Hydrol 2007;342:283–94. doi:10.1016/j.jhydrol.2007.05.029.
[17] Nordbotten JM, Celia MA, Bachu S. Injection and storage of CO_2 in deep saline aquifers: analytical solution for CO_2 plume evolution during injection. Transport Porous Med 2005;58:339–60.